



## Theoretical modeling of direct contact membrane distillation (DCMD): effects of operation parameters on flux

Parisa Moghaddam Kamrani<sup>a</sup>, Omid Bakhtiari<sup>b</sup>, Pezhman Kazemi<sup>c</sup>,  
Toraj Mohammadi<sup>a,\*</sup>

<sup>a</sup>Department of Chemical Engineering, Islamic Azad University, South Tehran Branch, Tehran, Iran, Tel. +98 21 77240496;

Fax: +98 21 77240496; emails: [parisa\\_mkamrani@yahoo.com](mailto:parisa_mkamrani@yahoo.com) (P. Moghaddam Kamrani), [torajmohammadi@iust.ac.ir](mailto:torajmohammadi@iust.ac.ir) (T. Mohammadi)

<sup>b</sup>Department of Chemical Engineering, Razi University, 67149-67346 Kermanshah, Iran, Tel. +98 8314283262;

email: [omidbakhtiari@iust.ac.ir](mailto:omidbakhtiari@iust.ac.ir) (O. Bakhtiari)

<sup>c</sup>Faculty of Pharmacy, Department of Pharmaceutical Technology and Biopharmaceutics, Medical College, Jagiellonian University, 30-688 Kraków, Poland, Tel. +48 786224645; email: [pezhman.kazemi@uj.edu.pl](mailto:pezhman.kazemi@uj.edu.pl) (P. Kazemi)

Received 10 March 2014; Accepted 22 August 2014

---

### ABSTRACT

In this research, a mathematical model for calculating and predicting flux through direct contact membrane distillation in flat-sheet membrane modules was presented. The membrane properties' and permeate and feed streams' main specifications were considered as model input parameters. The effects of simultaneous heat and mass transfer were investigated. The developed mathematical model was written in Visual Basic language based on heat and mass balances. The influences of process parameters such as temperature, flow rate, feed concentration, and membrane properties (pore size) on flux and temperature polarization coefficient were evaluated by the model. The modeling results were compared with some experimental data and good agreement was observed.

*Keywords:* Direct contact membrane distillation; Mathematical model; Flux prediction; Temperature polarization

---

### 1. Introduction

Membrane distillation (MD) is a combined thermal distillation and novel membrane separation process, in which only vapor molecules are transported through a porous hydrophobic membrane [1,2]. The driving force of MD process is quite different from other membrane processes and it is a vapor pressure difference between the two sides of membrane which is created by temperature difference across the membrane [3].

Today, MD is considered as a potential alternative to some traditional separation techniques and is believed to be effective in the fields of desalination, concentration of aqueous solution, etc. [1,2,4,5]. The difference between MD and other membrane separation techniques is the driving force of mass transfer through the membrane [6]. The characteristics of membranes used in MD must be micro-porous and un-wetted by process liquid and they should exhibit low resistance to mass transfer. Their pores are filled only by the vapor phase and no capillary condensation occurs inside the membrane pores.

---

\*Corresponding author.

There are various configurations developed to perform MD process which differ based on the nature of permeate side processing of the permeate, i.e. (1) direct contact membrane distillation (DCMD), (2) vacuum membrane distillation (VMD), (3) air gap membrane distillation (AGMD), and (4) sweeping gas membrane distillation (SGMD) [1,7]. Among various types of MD, DCMD in which the membrane is in direct contact only with liquid phases has been investigated extensively by different researchers and various theoretical models have been developed for flat-sheet and hollow fiber modules. Most of the models were developed assuming the process as one-dimensional using empirical heat and mass transfer equations. Two-dimensional theoretical models have been considered only in very few studies.

Most of the modeling works reported in literature are executable to a small number of given experimental variables. Accordingly, it is difficult to decisively validate the simplified models due to the limitations in available experimental data.

The dusty gas model has been applied first by Lawson and Lloyd to predict DCMD permeate flux where permeate flux was determined by considering heat transfer resistances in all parts and mass transfer resistance inside the membrane [3]. Phattaranawik et al. [8] developed a model which was able to study the effect of mass transfer on heat transfer rates and heat transfer coefficients. Monte Carlo simulation models have been carried out to study both heat and mass transfer in DCMD configuration [9–11] that it can simultaneously simulate MD permeate flux and temperatures at the membrane surfaces permitting evaluation of the temperature polarization coefficient (TPC). Bui et al. [12] proposed procedure for modeling transport processes in DCMD within a hollow fiber module, by adopting an analogy between heat and mass transfer in a dimensional analysis framework. Hwang et al. [13] proposed a two-dimensional model containing mass, energy, and momentum balance for predicting permeate flux for a flat-sheet module in DCMD system. The modeling results were compared with the experimental results of permeate fluxes from different velocity conditions and the error between the predicted results and the experimental results was in the range of  $\pm <10\%$ .

Ho et al. [14] developed a mathematical model for a heat transfer coefficient correction factor. The correlation is expressed as relative roughness and can be used for predicting the heat transfer coefficient for roughened-surface channels. This model allows the analysis of the temperature profiles inside DCMD module and reveals that even though considerable mass flux enhancement is obtained, the extent of

improved TPC is less due to the accompanying influence on fluid temperature change inside the module.

Michel et al. [15] performed different heat transfer prediction methods in combination with the three different forms of the Dusty Gas model for mass transport in comparison with experimental data in laminar and turbulent flow regimes under steady-state conditions and showed that the Knudsen-molecular diffusion transition model yields the best prediction.

In the current study, a mathematical model for DCMD by considering simultaneous heat and mass transfer balance in a flat-sheet module for pure water and NaCl solution is presented. This model was developed based on the characterizations of membrane and flow channel. The primary purpose of this model was to predict the membrane flux and investigate the influences of process parameters such as temperature, velocity, feed concentration, and membrane pore size on the permeate flux and TPC. Validity of the model was evaluated by performing a comparison between the experimental results presented in the literature with the results predicted by the present model.

## 2. Theoretical and mathematical model

MD is a complicated physical process in which both heat and mass transfers are involved [6,16].

Generally, the transport mechanism of MD can be summarized in: evaporation of water at the hot feed side of the membrane, penetration of water vapor through the membrane pores, and condensation of water vapor transported at the permeate side of the membrane [2,17]. Fig. 1 shows the schematic diagram for DCMD process [1].

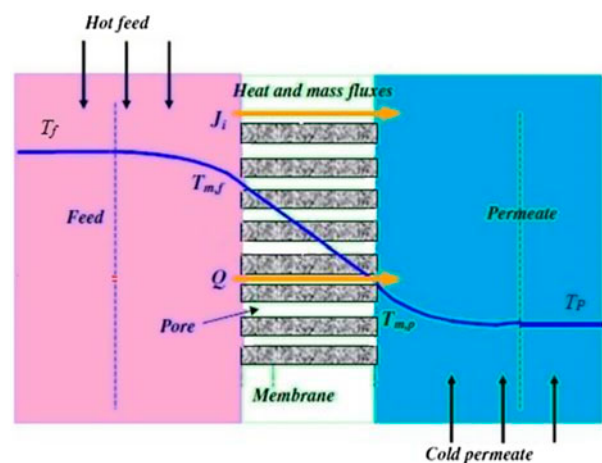


Fig. 1. Schematic diagram for DCMD [1].

### 2.1. Heat transfer

At the first stage, heat is transferred from the heated feed solution across the thermal boundary layer to the membrane surface. Then, the heat passes through the membrane in the form of vapor latent heat and heat conduction. Finally, the heat is removed from the cold side membrane surface through the boundary layer [18].

The heat flux for each step mentioned above can be expressed as follows:

For the feed side:

$$Q_f = \alpha_f (T_f - T_{fm}) \quad (1)$$

For the permeate side:

$$Q_p = \alpha_p (T_{pm} - T_p) \quad (2)$$

The difference between the bulk temperature and the temperature at the liquid–vapor interface or the membrane surfaces on both sides of the membrane is termed as “TPC” and assessed by:

$$TPC = (T_{fm} - T_{pm}) / (T_f - T_p) \quad (3)$$

where  $Q_f$  and  $Q_p$  are the heat flux (J/s),  $\alpha_f$  and  $\alpha_p$  are the convective heat transfer coefficients in feed and permeate sides (W/m<sup>2</sup>K),  $T_f$  and  $T_p$  are the feed and permeate temperatures (K), and  $T_{fm}$  and  $T_{pm}$  are the interface membrane temperatures in feed and permeate sides (K), respectively.

As TPC approaches unity, fluid dynamics of the system is good and the process is controlled by mass transfer through the membrane, while TPC approaches zero means that the system is designed poorly and the process is controlled by heat transfer through boundary layers. For almost all of the MD systems, TPC is in the range of 0.4–0.8 [1].

The heat flux depends on the film heat transfer coefficient in the boundary layer and the temperature difference between the feed bulk and the membrane surface.

Owing to the contribution of both evaporation and conduction, the total heat flux transferred through the membrane can be written as:

$$Q_f = (k_m / \delta) (T_{fm} - T_{pm}) + J \Delta H_{latent} \quad (4)$$

where  $J$  is the mass flux (mol/m<sup>2</sup>s),  $\Delta H_{latent}$  is the latent heat of vaporization (J/kg),  $\delta$  is the membrane thickness (m), and  $k_m$  is the thermal conductivity of

Table 1  
Thermal conductivity correlations

Model	Correlation	References
Isostrain	$k_m = \varepsilon k_g + (1 - \varepsilon) k_s$	[1,3,8]
Isostress	$k_m = \left[ \frac{\varepsilon}{k_g} + \frac{(1-\varepsilon)}{k_s} \right]^{-1}$	[1,8]
Flux law	$k_m = k_g \left[ \frac{1+(1-\varepsilon)\beta_{s-g}}{1-(1-\varepsilon)\beta_{s-g}} \right], \beta_{s-g} = \frac{k_s/k_g^{-1}}{k_s/k_g^{-2}}$	[8]

membrane material (W/m K). Various models have been considered to calculate thermal conductivity of the MD membrane as shown in Table 1 [1,8,18,19].

where  $\varepsilon$  is the porosity of the membrane, and  $k_s$  and  $k_g$  are the heat conductivity of the membrane material and the vapor that fills the pores, respectively. Isostrain model is often utilized for MD. Thermal conductivities of polytetrafluoroethylene (PTFE) and polypropylene (PP) are 0.25–0.27 and 0.11–0.16 (W/m K), respectively and air thermal conductivity value is 0.026 (W/m K) at 296 K [20].

Theoretically, heat transfer coefficients can be calculated using the following general expression [21].

$$\alpha_i = \frac{Nu \cdot k_w}{d_h} i = f, p \quad (5)$$

where Nu is the Nusselt number,  $K_w$  is the thermal conductivity of water, and  $d_h$  (m) is the hydraulic diameter for a flat-sheet module that can be expressed as:

$$d_h = \frac{2(D + W)}{(D \times W)} \quad (6)$$

where  $D$  is the depth and  $W$  is the width of flow channel.

There are a lot of empirical correlations for Nu, therefore choosing the best correlation for estimation of heat transfer coefficients completely depends on system hydrodynamics [20].

At steady state, for flat-sheet membrane modeling, heat balance can be expressed as:

$$Q = \alpha_f (T_f - T_{fm}) = (k_m / \delta) (T_{fm} - T_{pm}) + J \Delta H_{latent} = \alpha_p (T_{pm} - T_p) \quad (7)$$

where  $Q$  is the overall heat transfer.

### 2.2. Mass transfer

Mass transfer in the MD process includes three steps: firstly the hot feed is vaporized in the liquid/

gas interface, secondly the vapor is driven by the vapor pressure difference and diffuses from the hot interface to the permeate interface through the membrane pores, and thirdly the vapor is condensed into the permeate side stream [22].

The mass transfer through porous MD membranes can be interpreted by one of the three fundamental mechanisms: Knudsen diffusion, Molecular diffusion, and Poiseuille flow [23]. But the actual process is sometimes regulated by their combination known as transition mechanism. The Knudsen number ( $K_n$ ) is used to indicate the dominant mass transfer mechanism in the pores [1]:

$$K_n = l/d_m \quad (8)$$

where  $l$  is the mean free path of molecules and  $d_m$  is the mean pore size of membrane ( $\mu\text{m}$ ).

The mass transfer mechanism in porous membrane can be summarized as presented in Table 2, where  $P$ ,  $M$ , and  $K$  represent Poiseuille flow, molecular diffusion, and Knudsen diffusion, respectively.

In DCMD, the pressure difference at two sides of the membrane is zero when both the feed and permeate flows are under atmospheric pressure. In this case, the contribution of Poiseuille flow to mass transfer can be neglected. As pore size of the MD membranes is, in general, in the range of 0.2–1.0  $\mu\text{m}$  [7] and the mean free path of water vapor is 0.11  $\mu\text{m}$  at feed temperature of 60°C [22], according to Eq. (8),  $K_n$  is calculated in the range of 0.11–0.55. Therefore, Knudsen-Molecular transition diffusion is the dominating mass transfer mechanism within the membrane pores.

Therefore, mass transfer flux across the membrane can be expressed as [24]:

$$\frac{1}{J_{k-M}} = \frac{1}{J_k} + \frac{1}{J_M} \quad (9)$$

with:

$$J_k = \frac{-4d\varepsilon}{3t} \sqrt{\frac{1}{2\pi RMT}} \nabla P \quad (10)$$

Table 2

The influence of  $K_n$  on mass transfer through porous membrane [1]

$K_n < 0.01$	$0.01 < K_n < 1$	$K_n > 1$
M	M_K transition	K

$$J_M = \frac{-1}{1-x_A} \frac{\varepsilon D_{AB}}{tRT} \nabla P \quad (11)$$

And assuming ideal gas mixture in the membrane pores:

$$x_A = \frac{P_A}{P} \quad (12)$$

So the total vapor flux across the membrane as shown in Eq. (9) can be derived as [24]:

$$J = \frac{\varepsilon}{\Delta t} * PD_{AB} \ln \frac{\frac{P-P_{Tfm}}{PD_{AB}} + \frac{4}{3d} \sqrt{\frac{2\pi M}{RT}}}{\frac{P-P_{Tpm}}{PD_{AB}} + \frac{4}{3d} \sqrt{\frac{2\pi M}{RT}}} \quad (13)$$

where  $P_A$  is the partial pressure,  $P$  is the total (air + vapor) pressure (Pa),  $R$  is the universal gas constant (J/mol k),  $T$  is the mean temperature in the pore (K),  $M$  is the molecular mass (kg/mol k),  $t$  is the tortuosity factor of the membrane pores, and  $D_{AB}$  is the diffusion coefficient of vapor through air ( $\text{m}^2/\text{s}$ ) at temperature of 273–373 K which can be estimated from the following empirical equation [16]:

$$PD_{AB} = 1.895 * 10^{-5} T^{2.072} \quad (14)$$

Also,  $p_{Tpm}$  and  $p_{Tfm}$  are the vapor partial pressures (Pa) at the membrane-permeate and the membrane feed interfaces, respectively, which can be calculated using the Antoine's equation [3]:

$$p_{Ti} = \exp\left(A - \frac{B}{T+C}\right) \quad i = fm, pm \quad (15)$$

where  $p_{Ti}$  is the vapor pressure (Pa), and  $A$ ,  $B$ , and  $C$  are the experimental constants. For water,  $A = 238$ ,  $B = 3,841$ , and  $C = -45$ .

In Eq. (13), there are only two unknown variables, which are  $T_{fm}$  and  $T_{pm}$ . Therefore, if the interfacial temperature gradients on both sides of the membrane are calculated, the flux can be determined.

### 2.3. Solution procedure

The DCMD flow channel in the flat-sheet module was divided into small identical elements,  $\Delta x$ , and for each point (i), the differential equations of feed and permeate interfacial temperatures distributed along the membrane were written as:

$$\Delta T_{f,i} = T_{f,i+1} - T_{f,i} = \frac{-\alpha_{f,i}}{m_f C_{p,f}} (T_{f,i} - T_{fm,i}) \Delta x \quad (16)$$

$$\Delta T_{p,i} = T_{p,i+1} - T_{p,i} = \frac{\alpha_{p,i}}{m_p C_{p,p}} (T_{pm,i} - T_{p,i}) \Delta x \quad (17)$$

The overall heat transferred through the membrane at this point could be written as:

$$\Delta Q_i = U(T_{f,i} - T_{p,i}) \quad (18)$$

where  $U$  could be expressed as:

$$\frac{1}{U} = \frac{1}{\alpha_{p,i}} + \frac{1}{\alpha_{f,i}} + \frac{1}{\alpha_{m,i}} \quad (19)$$

$$\alpha_{m,i} = \frac{k_m}{\delta} + \frac{J_i \Delta H_{latent}}{T_{fm,i} - T_{pm,i}} \quad (20)$$

These differential equations were solved numerically using finite difference technique. This numerical solution was implemented using Visual Basic software.

The model was developed using the following assumptions:

- Operation is steady state;
- No heat from the module wall is transferred to the atmosphere;
- Specific heat of evaporation and condensation do not change with concentration;
- The membrane properties, such as thickness, porosity, pore size, and tortuosity, are constant;
- Temperature polarization effect isn't considered;

The characteristics (e.g. dimensions) of the channel and the membrane properties were considered as inputs. All physical properties of the feed and the permeate solutions were calculated at each point along the membrane length based on the bulk inlet and outlet temperatures. Thus, for each point, the membrane surface temperature and permeate flux were calculated.

### 3. Results and model validation

In order to evaluate the presented model prediction accuracy, the predicted values of transmembrane flux were compared with those of experimentally measured results of various membrane specifications, types, and operating conditions which are summarized in Table 3.

Table 3

Specifications and operating conditions used in DCMD experiments

Membrane type	3MA	3ME	PS22
Material	PP	PP	PP
Pore size (μm)	0.29	0.73	0.22
Thickness (μm)	91	79	150
Porosity (%)	60	85	70
Length (cm)	15.4	15.4	20
Feed temperature (°C)	20–80	20–80	30–60
Permeate temperature (°C)	20	20	20
Feed and permeate velocity (m/s)	1–2.2	1–2.2	0.5–2.5
References	[27]	[27]	[25]

#### 3.1. The effect of temperature

Most of the experimental data in the literatures describe the effect of feed temperature on the permeate flux. It is well known that the temperature in MD processes is the significant operating variable that affects the MD performance due to exponential increase of vapor pressure with temperature [16].

Figs. 2 and 3 represent effects of feed temperature on permeate flux for 3MA and 3ME membranes. The experimental data can be compared with the predicted results calculated for two kinds of PP flat-sheet membranes by the present model. The feed and the permeate flow rates were 63 (cm<sup>3</sup>/s) and the feed temperature range was between 30–80°C. Other characteristics parameters are shown in Table 2. The average deviation between the permeate fluxes predicted by the present model is 19.1% for 3MA membrane and 23.2% for 3ME membrane. The main reason for deviation between the predicted permeate fluxes

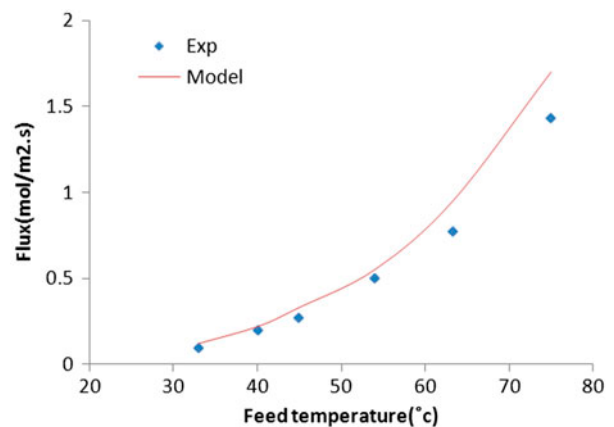


Fig. 2. MD pure water permeate flux as a function of feed temperature for 3MA membrane (Permeate temperature at 20°C).

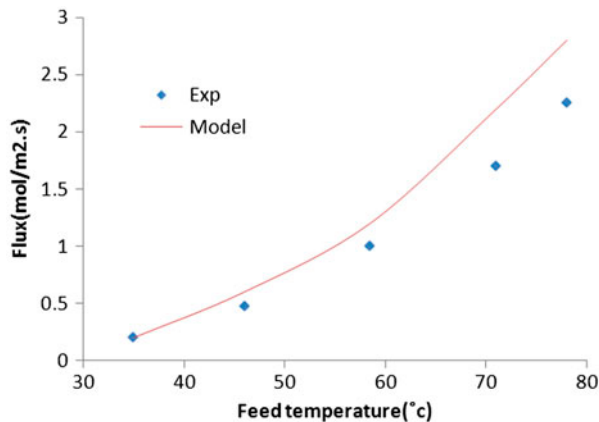


Fig. 3. MD pure water permeate flux as a function of feed temperature for 3ME membrane (Permeate temperature at 20°C).

and the experimental data at higher feed temperature can be due to the fact that at higher temperature, larger amount of heat is required to vaporize water at the membrane surface and thus the TPC increases and these lead to lower permeate fluxes, and since the effect of TPC isn't considered in this model the predicted results are overestimated. The other reasons that have less contribution are experimental error and different empirical equations, which are used for modeling. The reason for the differences in permeation fluxes for 3MA and 3ME membranes is due to the different characteristics of membranes, such as porosity, pore size, and thickness.

The comparison between experimental data reported by Cath et al. [25] and the results predicted by the model are shown in Fig. 4. The membrane was

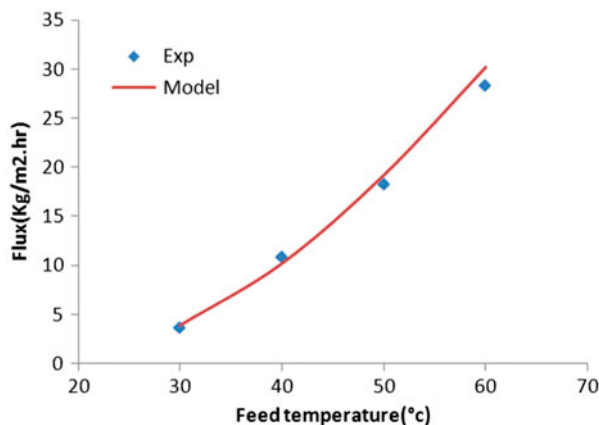


Fig. 4. MD pure water permeate flux as a function of feed temperature for PS22 membrane (Permeate temperature at 20°C and velocity at 1.75 m/s).

made up of PP. The permeate stream temperature was maintained at 20°C and feed and permeate stream velocities were both maintained at 1.75 m/s. Feed salt concentration was 0.6 g/l NaCl. Other characteristics parameters are shown in Table 2.

It can be noticed that the permeate flux predicted by the present model is in a good agreement with the experimental data with an average deviation of about 6.4%. The membrane characteristics, such as pore size, thickness, and porosity, play very important role on permeation flux. In fact, these values were supplied by the manufacturer and there is a level of uncertainty [16].

Figs. 5 and 6 show the effect of permeate temperature on permeate flux for 3MA and 3ME membranes, respectively. The experimental data and simulation

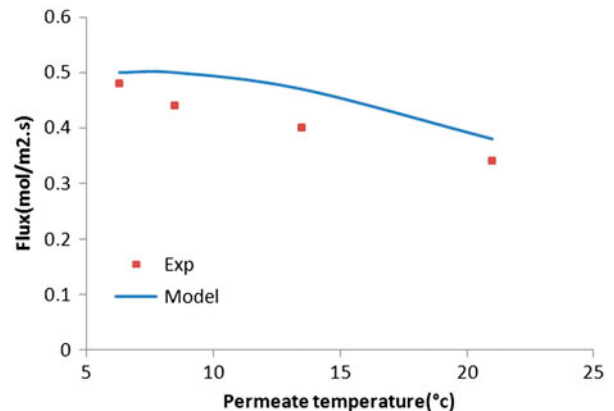


Fig. 5. MD pure water permeate flux as a function of permeate temperature for 3ME membrane (Feed temperature at 41°C).

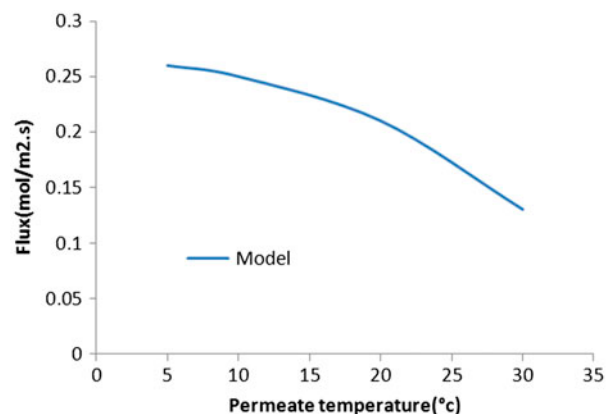


Fig. 6. Simulated pure water permeate flux as a function of permeate temperature for 3MA membrane (Feed temperature at 41°C).

result for 3ME membrane can be compared. As observed, permeate flux decreases with increasing permeate temperature and this is due to the reduction of the MD process driving force.

Compared with feed temperature, permeate temperature has less effect on permeate flux. This can be attributed to the different extent that vapor pressure changes with temperature. At higher feed temperature, vapor pressure changes significantly with increasing feed temperature and this makes a more significant driving force, while at lower permeate temperature vapor pressure changes, relatively, slowly with increasing feed temperature and this makes a less significant driving force. Although increasing feed temperature can effectively enhance permeate flux in DCMD, the large temperature difference may also improve heat conduction from the membrane module to the atmosphere, which isn't good for heat transfer. From this viewpoint, there should be a trade-off between permeate flux and thermal efficiency [26].

The effect of feed temperature on TPC for 3MA, 3ME, and PS22 membranes is plotted in Figs. 7 and 8. The results generally show that TPC decreases with increasing feed temperature. TPC for 3MA membrane, in the range of studied temperatures, is higher than that of 3ME membrane. This can be due to the fact that thickness of 3MA membrane is higher than that of 3ME membrane and by increasing the membrane thickness mass transfer resistance increases and as a result TPC increases and permeate flux decreases.

### 3.2. Effect of velocity

The effect of flow velocity on permeate flux in DCMD was studied as shown in Figs. 9 and 10. In

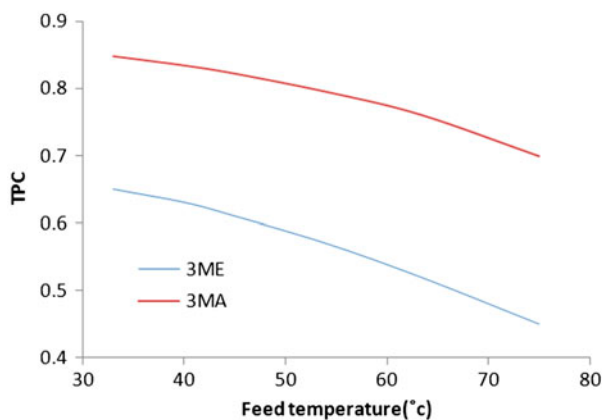


Fig. 7. Effect of feed temperature on TPC of pure water for 3MA and 3ME membranes (Permeate temperature at 20°C).

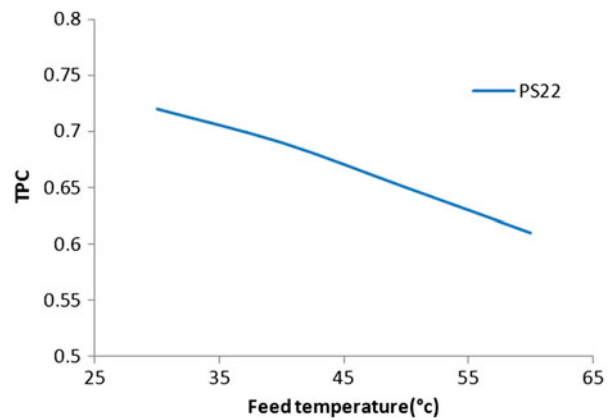


Fig. 8. Effect of feed temperature on TPC of pure water for PS22 membrane (Permeate temperature at 20°C).

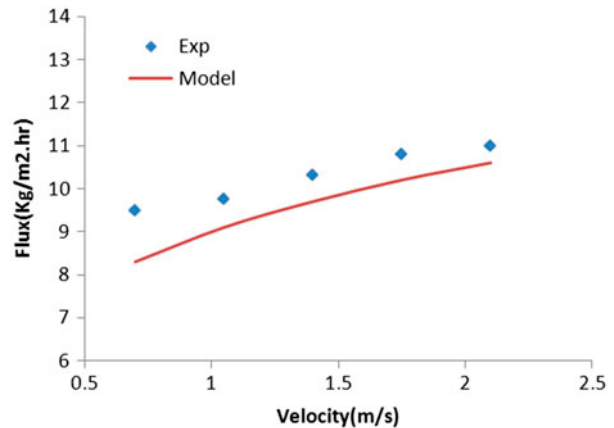


Fig. 9. Effect of velocity on permeate flux for PS2 membrane (Feed temperature at 40°C and permeate temperature at 20°C).

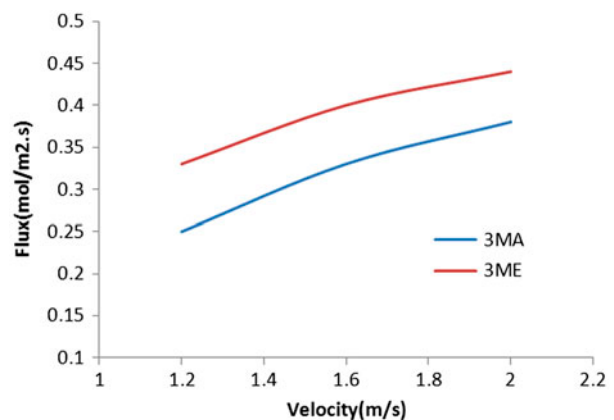


Fig. 10. Effect of velocity of pure water on permeate flux for 3MA and 3ME membranes (Feed temperature at 40°C and permeate temperature at 20°C).

Fig. 9, the experimental data of Cath et al. [25] with the results calculated by the present model was compared. The both streams velocity (feed and permeate) were equal, feed and permeate temperature was contain in 40 and 20°C, respectively. The average deviation between them is about 7.1%. It can be observed that permeate flux increases by increasing flow velocity. This is due to the fact that increasing flow velocity reduces heat transfer resistance within the boundary layers and thus permeate flux increases.

Figs. 11 and 12 shows the effect of flow velocity on TPC for 3MA, 3ME, and PS22 membranes. It can be observed that with increasing velocity, TPC increases. As mentioned, increasing TPC reduces heat transfer resistance within boundary layers and this increases permeate flux [16].

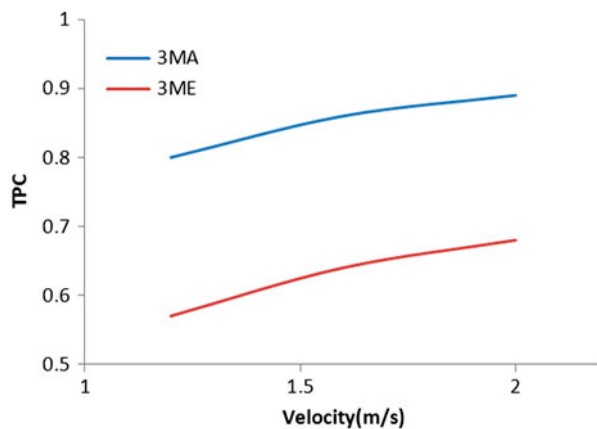


Fig. 11. Effect of flow velocity on TPC for 3MA and 3ME membranes (Feed temperature at 40°C and permeate temperature at 20°C).

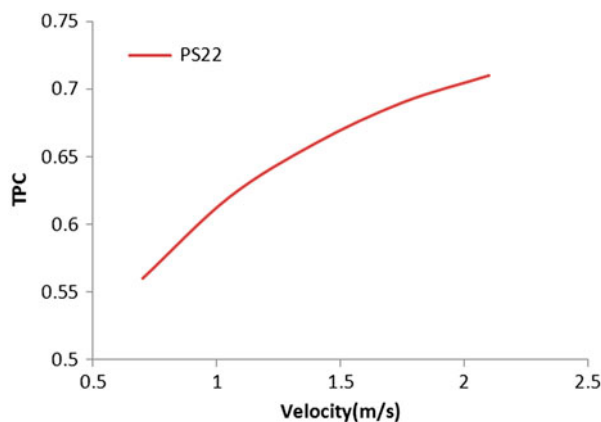


Fig. 12. Effect of flow velocity on TPC for PS22 membrane (Feed temperature at 40°C and permeate temperature at 20°C).

### 3.3. Effect of feed salt NaCl concentration

The estimated results by the present model have been compared with the experimental results reported by Lawson and Lloyd [27] for 3MA membrane. The feed and permeate temperature were 45 and 20°C, respectively, and the feed and the permeate flow rates were 63 cm<sup>3</sup>/s. As observed in Fig. 13, permeate flux decreases slightly as feed salt (NaCl) concentration increases. This can be attributed to the fact that increasing feed salt concentration reduces partial vapor pressure of water over the membrane surface and this reduces mass transfer driving force. Average deviation is about 16.8%. The overestimation is due to the fact that in higher NaCl concentration, solution viscosity is higher, and as a result, heat transfer by both conduction and convection decreases and thus the predicted permeate flux is higher than the experimental value.

### 3.4. Effect of membrane pore size

For gas transport through porous medium, pore size influences permeability. The effect of pore size (pore diameter) on permeate flux of DCMD can, theoretically, be predicted based on the mathematical model discussed above, and the results are presented and compared for 3ME membrane at 40 and 60°C in Fig. 14. It can be observed that pore size has slight influence on permeate flux when pore diameter is larger than 0.4 μm. A considerable permeate flux change can be observed only when pore diameter is less than 0.4 μm.

As mentioned before, mass transfer through porous membranes in DCMD is often regulated by

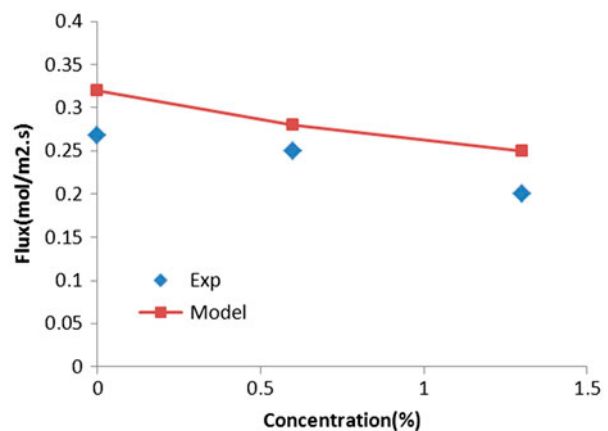


Fig. 13. Effect of NaCl concentration on permeate flux for 3MA membrane (Feed temperature at 45°C and permeate temperature at 20°C).

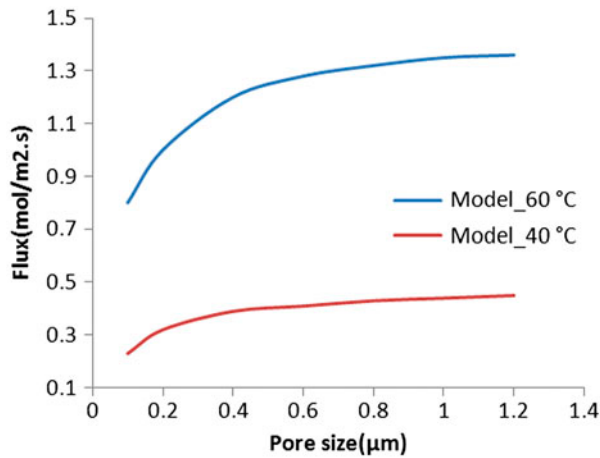


Fig. 14. Effect of membrane pore size on permeate flux for 3ME membrane (Feed and permeate flow rate at  $63 \text{ cm}^3/\text{s}$  and permeate temperature at  $20^\circ\text{C}$ ).

Knudsen-molecular diffusion transition. These two resistances to mass transfer are combined in series. When pore diameter is less than  $0.4 \text{ }\mu\text{m}$ , molecular-wall collision (or Knudsen diffusion) dominates mass transfer process. Therefore, pore size is an important factor (as indicated in Eq. (10)). However, by increasing pore size, molecular-wall collision (or Knudsen diffusion) becomes less important in mass transfer process. Larger the pore size, lesser the opportunity for vapor molecules to collide with the pore wall. In this case, Knudsen diffusion mechanism becomes less important. On the other hand, the less molecule-wall collision the more molecule-molecule collision within the membrane pores. However, molecular diffusion mechanism has no relation with pore size, as indicated in Eq. (11) [26].

#### 4. Conclusion

A new simultaneous heat and mass transfer model for flat-sheet DCMD configuration was presented in this study. The influence of the temperature, velocity, and the salt concentration of the feed along the module on the permeate flux are evaluated by the present model and compared with the experimental data collected from the literature and showed reasonable agreement. The model predictions showed that:

- For lower feed temperature conditions, modeling results are better than those for higher feed temperatures compared with experimental results.
- Under the same hydraulic flows, the higher feed temperatures lead to the lower TPCs because the greater heat flux leads to the higher permeate flux.

- For the bigger pore size, there is no significant effect on permeate flux.
- Increasing feed temperature is more effective than decreasing permeate temperature on permeate flux.
- Flux decreased with increase in the NaCl concentration that was attributed to the fact that increasing feed salt concentration reduces partial vapor pressure of water over the membrane surface and this reduces mass transfer driving force.

#### Nomenclature

$\alpha_f, \alpha_p$	—	heat transfer coefficient on hot and cold sides ( $\text{W}/\text{m}^2 \text{K}$ )
$C_{p,f}, C_{p,p}$	—	specific heat of feed and permeate ( $\text{J}/\text{kg K}$ )
$D$	—	membrane depth (m)
$D_{AB}$	—	diffusivity of water vapor (A) relative to air (B) ( $\text{m}^2/\text{s}$ )
$d$	—	pore size ( $\mu\text{m}$ )
$d_m$	—	mean pore size ( $\mu\text{m}$ )
$d_h$	—	hydraulic diameter (m)
$\varepsilon$	—	membrane porosity
$\Delta H_{latent}$	—	latent heat of water vaporization ( $\text{J}/\text{kg}$ )
$J$	—	vapor flux ( $\text{mol}/\text{m}^2 \text{s}$ )
$k_g$	—	air thermal conductivity ( $\text{W}/\text{m K}$ )
$k_m$	—	thermal conductivity of membrane ( $\text{W}/\text{m K}$ )
$k_s$	—	solid thermal conductivity ( $\text{W}/\text{m K}$ )
$k_w$	—	water thermal conductivity ( $\text{W}/\text{m K}$ )
$l$	—	the mean free path of the transferred gas molecule ( $\mu\text{m}$ )
$L$	—	module length (m)
$M$	—	molecular weight of water ( $\text{kg}/\text{mol}$ )
$m_f, m_p$	—	mass flow rates of feed and permeate streams ( $\text{kg}/\text{s}$ )
$\delta$	—	thickness ( $\mu\text{m}$ )
$p_{T_{fm}}, p_{T_{pm}}$	—	vapor pressure at $T_{fm}$ and $T_{pm}$ (Pa)
$P_A$	—	partial pressure (Pa)
$Q_f, Q_p$	—	total heat transfer of feed and permeate ( $\text{J}/\text{s}$ )
$R$	—	universal gas constant ( $\text{J}/\text{mol K}$ )
$t$	—	pore tortuosity
$T_f, T_p$	—	permeate and feed bulk temperatures (K)
$T_{fm}, T_{pm}$	—	feed and permeate temperatures at liquid–vapor interface (K)
$T$	—	mean temperature in the pore (K)
$U$	—	global heat transfer coefficient ( $\text{mol}/\text{pa m}^2 \text{s}$ )
$W$	—	membrane width (m)
$x$	—	$x$ direction (m)

#### References

[1] M. Khayet, Membranes and theoretical modeling of membrane distillation: A review, *Adv. Colloid Interface Sci.* 164 (2011) 56–88.

- [2] M.S. El-Bourawi, Z. Ding, R. Ma, M. Khayet, A framework for better understanding membrane distillation separation process, *J. Membr. Sci.* 285 (2006) 4–29.
- [3] K.W. Lawson, D.R. Lloyd, Membrane distillation, *J. Membr. Sci.* 124 (1997) 1–25.
- [4] M. Khayet, Treatment of radioactive wastewater solutions by direct contact membrane distillation using surface modified membranes, *Desalination* 321 (2013) 60–66.
- [5] T. Mohammadi, P. Kazemi, Taguchi optimization approach for phenolic wastewater treatment by vacuum membrane distillation, *Desalin. Water Treat.* 52 (2014) 1341–1349.
- [6] A.M. Alklaibi, N. Lior, Heat and mass transfer resistance analysis of membrane distillation, *J. Membr. Sci.* 282 (2006) 362–369.
- [7] A.M. Alklaibi, N. Lior, Membrane-distillation desalination: Status and potential, *Desalination* 171 (2005) 111–131.
- [8] J. Phattaranawik, R. Jiratananon, A.G. Fane, Heat transport and membrane distillation coefficients in direct contact membrane distillation, *J. Membr. Sci.* 212 (2003) 177–193.
- [9] M. Khayet, A.O. Imdakm, T. Matsuura, Monte Carlo simulation and experimental heat and mass transfer in direct contact membrane distillation, *Int. J. Heat Mass Transfer* 53 (2010) 1249–1259.
- [10] A.O. Imdakm, T. Matsuura, A Monte Carlo simulation model for membrane distillation processes: Direct contact (MD), *J. Membr. Sci.* 237 (2004) 51–59.
- [11] F. Laganà, G. Barbieri, E. Drioli, Direct contact membrane distillation: Modelling and concentration experiments, *J. Membr. Sci.* 166 (2000) 1–11.
- [12] V.A. Bui, L.T.T. Vu, M.H. Nguyen, Modelling the simultaneous heat and mass transfer of direct contact membrane distillation in hollow fibre modules, *J. Membr. Sci.* 353 (2010) 85–93.
- [13] H.-J. Hwang, K. He, S. Gray, J. Zhang, S. Moon, Direct contact membrane distillation (DCMD): Experimental study on the commercial PTFE membrane and modeling, *J. Membr. Sci.* 371 (2011) 90–98.
- [14] C.-D. Ho, H. Chang, C.-L. Chang, C.-H. Huang, Theoretical and experimental studies of flux enhancement with roughened surface in direct contact membrane distillation desalination, *J. Membr. Sci.* 433 (2013) 160–166.
- [15] B. Michel, O. Andrijesdóttir, C.-L. Ong, M. Nabavi, S. Paredes, A.S. Khalil, D. Poulikakos, An experimentally optimized model for heat and mass transfer in direct contact membrane distillation, *Int. J. Heat Mass Transfer* 66 (2013) 855–867.
- [16] M. Qtaishat, T. Matsuura, B. Kruczek, M. Khayet, Heat and mass transfer analysis in direct contact membrane distillation, *Desalination* 219 (2008) 272–292.
- [17] A. Alkudhiri, N. Darwish, N. Hilal, Membrane distillation: A comprehensive review, *Desalination* 287 (2012) 2–18.
- [18] R.W. Schofield, A.G. Fane, C.J.D. Fell, Heat and mass transfer in membrane distillation, *J. Membr. Sci.* 33 (1987) 299–313.
- [19] L. Martinez-Diez, M.I. Vázquez-González, Temperature and concentration polarization in membrane distillation of aqueous salt solutions, *J. Membr. Sci.* 156 (1999) 265–273.
- [20] E. Curcio, E. Drioli, Membrane distillation and related operations—A review, *Sep. Purif. Rev.* 34 (2005) 35–86.
- [21] R.W. Serth, *Process Heat Transfer: Principles and Applications*, Elsevier Academic Press CY, Amsterdam, London, 2007.
- [22] J. Zhang, N. Dow, M. Duke, E. Ostarcevic, J.-D. Li, S. Gray, Identification of material and physical features of membrane distillation membranes for high performance desalination, *J. Membr. Sci.* 349 (2010) 295–303.
- [23] W. Kast, C.R. Hohenthanner, Mass transfer within the gas-phase of porous media, *Int. J. Heat Mass Transfer* 43 (2000) 807–823.
- [24] J. Phattaranawik, R. Jiratananon, A.G. Fane, C. Halim, Effect of pore size distribution and air flux on mass transport in direct contact membrane distillation, *J. Membr. Sci.* 215 (2003) 75–85.
- [25] T.Y. Cath, V.D. Adams, A.E. Childress, Experimental study of desalination using direct contact membrane distillation: A new approach to flux enhancement, *J. Membr. Sci.* 228 (2004) 5–16.
- [26] Z. Lei, B. Chen, Z. Ding, Membrane distillation, in: Z. Lei, B. Chen, Z. Ding (Eds.), *Special Distillation Processes*, Elsevier Science, Amsterdam, 2005, pp. 241–319.
- [27] K.W. Lawson, D.R. Lloyd, Membrane distillation. II. Direct contact MD, *J. Membr. Sci.* 120 (1996) 123–133.